arXiv:1201.4903v1 [math.NA] 24 Jan 2012

UNIVERSAL MESHES: A NEW PARADIGM FOR COMPUTING WITH NONCONFORMING TRIANGULATIONS

RAMSHARAN RANGARAJAN AND ADRIÁN J. LEW

Abstract. We describe a method for discretizing planar C^2-regular domains immersed in nonconforming triangulations. The method consists in constructing mappings from triangles in a background mesh to curvilinear ones that conform exactly to the immersed domain. Constructing such a map relies on a novel way of parameterizing the immersed boundary over a collection of nearby edges with its closest point projection. By interpolating the mappings to curvilinear triangles at select points, we recover isoparametric mappings for the immersed domain defined over the background mesh. Indeed, interpolating the constructed mappings just at the vertices of the background mesh yields a fast meshing algorithm that involves only perturbing a few vertices near the boundary.

For the discretization of a curved domain to be robust, we have to impose restrictions on the background mesh. Conversely, these restrictions define a family of domains that can be discretized with a given background mesh. We then say that the background mesh is a *universal mesh* for such a family of domains. The notion of universal meshes is particularly useful in free/moving boundary problems because the same background mesh can serve as the universal mesh for the evolving domain for time intervals that are independent of the time step. Hence it facilitates a framework for finite element calculations over evolving domains while using a fixed background mesh. Furthermore, since the evolving geometry can be approximated with any desired order, numerical solutions can be computed with high-order accuracy. We demonstrate these ideas with various numerical examples.

Key words. universal meshes, meshing, background mesh, immersed boundary, closest point projection

AMS subject classifications. 65N30, 68U05, 65M50, 65N50

1. Introduction. Finite element methods commonly handle evolving domains in one of two ways — either the changing domain is remeshed at each instant/update, or it is immersed in a background mesh and approximated within it. We introduce a novel approach here that inherits the conceptual simplicity of the former and the computational efficiency of the latter. We describe a method for discretizing sufficiently smooth planar domains *using* a given background triangulation, provided some conditions are met. The method consists in constructing mappings from triangles in a background mesh to curvilinear ones that conform exactly to the immersed domain. As an example, consider simulating a problem in which rigid blades physically mix fluid in a closed container. As the blades rotate, the region of the container occupied by the fluid changes. We can now discretize the evolving fluid domain by merely perturbing vertices and edges of the *same* background mesh. Precisely because the same background mesh is utilized for all positions of the propeller, we term it a *universal mesh* for the fluid. Since connectivities of triangles remain unaltered and no new vertices are introduced, sparse patterns of data structures involved in the problem can also be retained.

The basic idea: The key idea in constructing conforming discretizations for an immersed domain consists of a two-step procedure to perturb edges and vertices in its background mesh. We identify triangles in the background mesh with at least one vertex inside the curved domain. Edges belonging to this collection having both vertices outside the domain are mapped onto the boundary with its closest point projection. Then we relax away from the boundary a few vertices that lie inside the domain and close to the boundary. For a certain class of background meshes, these steps enable us to construct a homeomorphism between the union of selected triangles in the background mesh and the the domain. In other words, this construction yields

a conforming curvilinear discretization for the immersed domain.

There are no conformity requirements on the background mesh; for instance, none of its vertices need to lie on the boundary. The resulting algorithmic advantages are significant, especially for problems with evolving domains. Such problems are ubiquitous, including ones with interaction between fluids and solids, problems with free boundaries and moving interfaces, domains with propagating cracks and problems with phase transformations. Various numerical schemes have been proposed for such applications, see references [3, 10, 19, 20, 27] for a representative few. The spirit of this article, as evidenced by the examples presented, is to immerse such evolving geometries in a universal mesh and update its spatial discretization as necessary.

Numerical methods that adopt nonconforming meshes have been formulated in various ways. For instance, by re-triangulating elements near the boundary and with cut/trimmed cells [18, 24]; by treating immersed boundaries and interfaces via constraints using penalty [1], Lagrange multipliers [6] and Nitsche's method [14]; or by enriching the space of solutions near the boundary as done in extended finite element methods and discontinuous Galerkin-based methods [27, 16]. One of the challenges in these methods is achieving optimal accuracy with high-order interpolations. Almost without exception, these methods resort to a polygonal approximation for the immersed domain. Such approximations suffice in low order methods, in which the solution is approximated by piecewise constant or affine functions [16, 22]. To construct high-order methods, it is imperative to approximate the immersed geometry sufficiently well over the background mesh.

With conforming curvilinear discretizations for immersed domains, we can construct curved finite elements with optimal convergence rates given only nonconforming background meshes (§3). Alternately, by interpolating the mappings to curvilinear triangles at select points, we recover isoparametric mappings defined over the background mesh, as discussed in §4. Rather than discretizing a curved domain exactly, isoparametric mappings provide a systematic way of constructing *sufficiently accurate* approximations in which curved edges interpolate the boundary at select points/nodes. Both exactly conforming and isoparametric elements enable high-order convergence rates (see §3.2). The former type of elements can be particularly advantageous in problems sensitive to boundary conditions. One such problem is that of a simply supported circular plate in bending [2]. In §4.2, we show that the accuracy of its numerical solution can be sensitive to how well curved boundaries are represented.

The construction for curved domains given here are inspired by the well known mappings proposed in references [13, 15, 17, 26, 28]. The constructions in these articles assume as a point of departure, (i) a conforming mesh for the curved domain, and (ii) a parametrization for the curved boundary over edges that interpolate it. By admitting nonconforming meshes and not relying on a specific representation for the boundary, we relax both assumptions. Hence we generalize these known constructions to a larger class of meshes and amenable to general boundary representations. For example, the boundary can be given parametrically as a collection of splines, or implicitly as the zero level set of a function. We only require a way to compute the closest point projection sufficiently close to the boundary.

In the special case when the mappings to curvilinear triangles are interpolated just at vertices in the background mesh, we get a conforming mesh for the immersed domain. The resulting "meshing algorithm" is very fast, since it only involves perturbing vertices. For simplicity, we present the meshing algorithm first, in §2, by defining affine mappings that perturb vertices of the background mesh near the immersed

boundary. In contrast, conforming curvilinear discretizations, discussed in §3, are constructed by mapping certain *edges*, rather than just vertices, onto the boundary.

It is common knowledge that perturbing vertices in a background mesh *can* yield a conforming mesh for an immersed domain. The challenge, though, is making such algorithms robust. An algorithm specific to the case of domains immersed in rectangular grids is described in [5]. The closest point projection has also been used to locally modify Cartesian grids near the boundary, as done in [12, 25] although the authors do not consider when their approach could fail.

In §2.1, we list sufficient conditions for our meshing algorithm to be robust. We assume that the curved domain is C^2-regular, and we have to *restrict the class of background meshes* for a given domain. In particular, we require that the background mesh be sufficiently refined and that certain angles in triangles near the boundary be acute. With these assumptions, we analyzed the restriction of the closest point projection to the edges whose vertices are projected onto the immersed boundary in [21]. We proved that this mapping is in fact a homeomorphism onto the boundary. As we discuss in §5, such a result and a possibly smaller mesh size ensures that moving vertices of the background mesh in the way we do in the meshing algorithm will not result in degenerate, inverted, or overlapping triangles, and in general, avoids tangled meshes. For instance, a refined background mesh of equilateral triangles is guaranteed to mesh a smooth domain immersed in it. We cannot however make the same claim with a background mesh of right angled triangles, because such a mesh may not satisfy the condition on angles. The conditions required for the success of the meshing algorithm along with possibly smaller mesh size near the boundary also ensure that the mappings to conforming and isoparametric curved elements are well defined as well.

2. From background meshes to conforming meshes. We begin by illustrating the steps to determine a conforming mesh for a planar curved domain Ω immersed in a background triangulation $\mathcal{T}_h$, where h denotes the mesh size. We assume that Ω is an open set and denote $\Omega^c = \mathbb{R}^2 \setminus \Omega$. By Ω being *immersed* in $\mathcal{T}_h$, we mean that the set triangulated by $\mathcal{T}_h$ contains $\overline{\Omega}$. To ensure that the resulting mesh for Ω is valid, we require certain assumptions on Ω and $\mathcal{T}_h$. They are stated in §2.1 and discussed in §5.

Table 2.1: Steps in the meshing algorithm

Step 1: Identify vertices in the background mesh $\mathcal{T}_h$ that lie in Ω (square markers) and in Ω^c (circular markers) respectively. Omit triangles with no vertices in Ω.	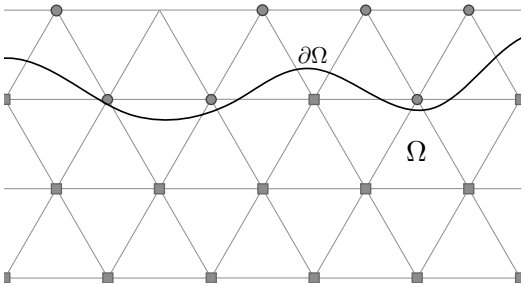

Step 2: Identify *positively cut triangles* in $\mathcal{T}_h$ — triangles with precisely one vertex in Ω. These are shaded in gray. In each such triangle, check that the angle at its vertex in Ω^c closest to $\partial\Omega$ is smaller than $90°$. These angles are labeled ϑ in the adjacent figure.

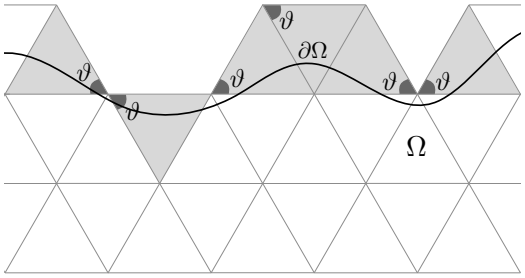

Step 3: A *positive edge* is the edge of a positively cut triangle joining its vertices in Ω^c. These edges are shown in black. Map vertices of positive edges to their closest point on the boundary $\partial\Omega$.

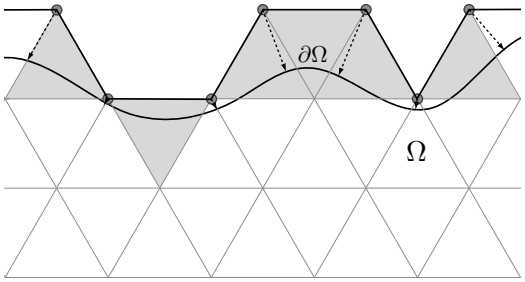

Step 4: Identify vertices in Ω that lie close to $\partial\Omega$, such as the ones shown by triangular markers. Perturb these vertices away from $\partial\Omega$ using the mapping $\mathfrak{p}_h$ in (2.1).

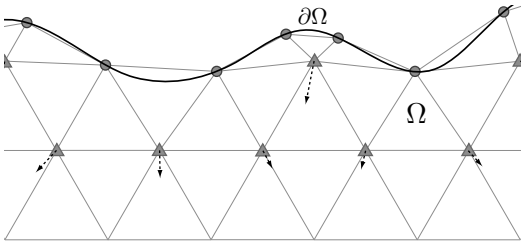

Final Mesh

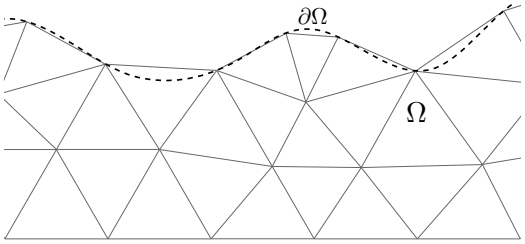

The mapping for relaxing vertices away from the boundary is given by

$$\mathfrak{p}_h(x) = \begin{cases} x - \eta h \left(1 + \frac{\phi(x)}{r}\right) \nabla\phi(x) & \text{if } -r < \phi(x) < 0, \\ x & \text{otherwise,} \end{cases} \tag{2.1}$$

where ϕ is the signed distance function to $\partial\Omega$ defined below in §2.4, $\eta \in (0,1)$ and r equals a few multiples of the mesh size h. We discuss the choice of η and r in §2.4 as well.

The meshing algorithm in Table 2.1 is succinctly summarized as a piecewise affine mapping over triangles in $\mathcal{T}_h$. To this end, let $\pi : \mathbb{R}^2 \to \partial\Omega$ denote the closest point

projection onto $\partial\Omega$, and identify the collections of triangles

$$\mathcal{T}_h^i = \{K \in \mathcal{T}_h \,:\, \phi \geq 0 \text{ at precisely } i \text{ vertices of } K\} \tag{2.2}$$

for $i = 0, 1, 2, 3$. Consider a triangle $K \in \mathcal{T}_h^{0,1,2}$ with vertices $\{u, v, w\}$ ordered such that $\phi(u) \geq \phi(v) \geq \phi(w)$. Denote the barycentric coordinates of $x \in \overline{K}$ by $(\lambda_u, \lambda_v, \lambda_w)$ so that $x = \lambda_u\, u + \lambda_v\, v + \lambda_w\, w$ and $\lambda_u + \lambda_v + \lambda_w = 1$. The algorithm in Table 2.1 maps $x \mapsto M_K^h(x)$ defined as

$$M_K^h(x) = \begin{cases} \lambda_u \mathfrak{p}_h(u) + \lambda_v \mathfrak{p}_h(v) + \lambda_w \mathfrak{p}_h(w) & \text{if } K \in \mathcal{T}_h^0, \\ \lambda_u \pi(u) + \lambda_v \mathfrak{p}_h(v) + \lambda_w \mathfrak{p}_h(w) & \text{if } K \in \mathcal{T}_h^1, \\ \lambda_u \pi(u) + \lambda_v \pi(v) + \lambda_w \mathfrak{p}_h(w) & \text{if } K \in \mathcal{T}_h^2. \end{cases} \tag{2.3}$$

To refer to the angles checked in step 2 in Table 2.1, we introduce the terms *proximal vertices* and *conditioning angles*. The proximal vertex of a positively cut triangle is the vertex of its positive edge closer to $\partial\Omega$. If both vertices of the positive edge are equidistant from $\partial\Omega$, the one containing the smaller interior angle is chosen as the proximal vertex. If the angles are equal as well, the choice is arbitrary. The conditioning angle of a positively cut triangle is the interior angle at its proximal vertex. Hence in step 2 of Table 2.1, we require that each positively cut triangle have an acute conditioning angle.

2.1. Sufficient conditions for a valid mesh. We require a few assumptions to guarantee that the meshing algorithm in Table 2.1 yields a valid mesh for the immersed domain Ω. By a valid mesh we mean a triangulation of a polygon Ω_h made of triangles with diameters smaller or equal to h, such that the vertices of Ω_h lie on $\partial\Omega$, and Ω_h approximates Ω as $h \searrow 0$[1]. We require that

(a) the domain Ω be C^2-regular,
(b) that Ω be immersed in $\mathcal{T}_h$, i.e., $\overline{\Omega} \subset \cup_{K \in \mathcal{T}_h} \overline{K}$,
(c) the conditioning angle in each positively cut triangle in $\mathcal{T}_h$ be strictly smaller than $90°$, and
(d) the triangulation $\mathcal{T}_h$ be sufficiently refined in the vicinity of $\partial\Omega$.

A precise definition of C^k-regular domains is given in [21]. For our purposes, it suffices to note that Ω is C^2-regular if the signed distance function to $\partial\Omega$ is C^2 in a neighborhood of $\partial\Omega$. Assumption (d) requires that the mesh size be small near $\partial\Omega$. By this we mean that if triangle $K \in \mathcal{T}_h$ lies near $\partial\Omega$, then its diameter h_K should be smaller than a value that depends on the local curvature and feature size of $\partial\Omega$, among others. Explicit estimates for the required mesh size near $\partial\Omega$ are essential to automate the algorithm. However, we do not provide such estimates here. We do briefly mention how to construct adaptively refined background meshes satisfying the acute conditioning angle requirement (c) in §2.4. We discuss the rationale behind these assumptions later in §5.

2.2. An illustrative example. An example that uses the meshing algorithm is shown in Fig. 2.1. The curved domain to be meshed is the one shown in Fig. 2.1a. It is C^2-regular because its boundary is a collection of cubic splines. It is immersed in a background mesh of equilateral triangles. Hence the conditioning angle equals $60°$ and the check in step 2 in Table 2.1 (also assumption (c) in §2.1) is trivially satisfied. In Fig. 2.1a, the 2382 triangles in $\mathcal{T}_h^{0,1,2}$ are shaded in gray. Triangles

[1] At least we need to have $|\Omega_h \setminus \Omega \cup \Omega \setminus \Omega_h| \to 0$ and $\text{distance}(\partial\Omega_h, \partial\Omega) \to 0$ as $h \searrow 0$.

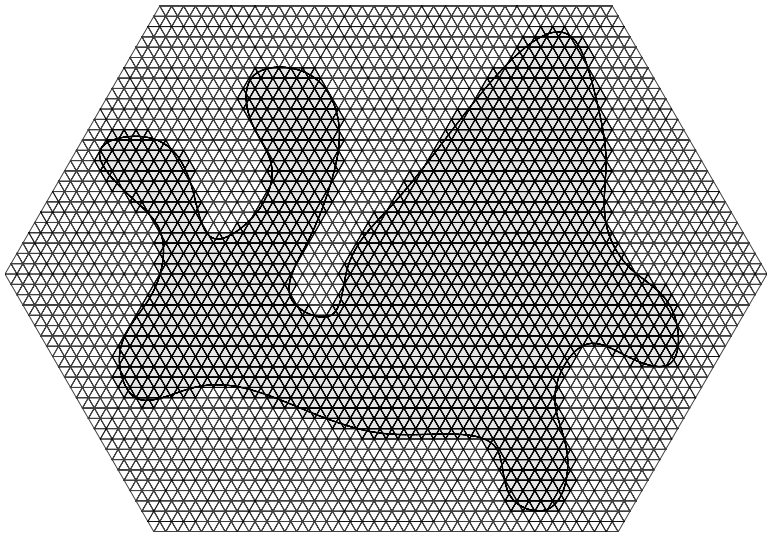

(a) A curved domain is immersed in a background mesh of equilateral triangles. The boundary of the domain shown is composed of 41 cubic splines. Its is therefore C^2-regular. Since all interior angles of triangles in the background mesh equal 60°, the conditioning angle also equals 60°. Triangles with at least one vertex inside the domain (i.e., triangles in $\mathcal{T}_h^{0,1,2}$) are shaded in gray. These triangles are mapped to a conforming mesh for the immersed domain.

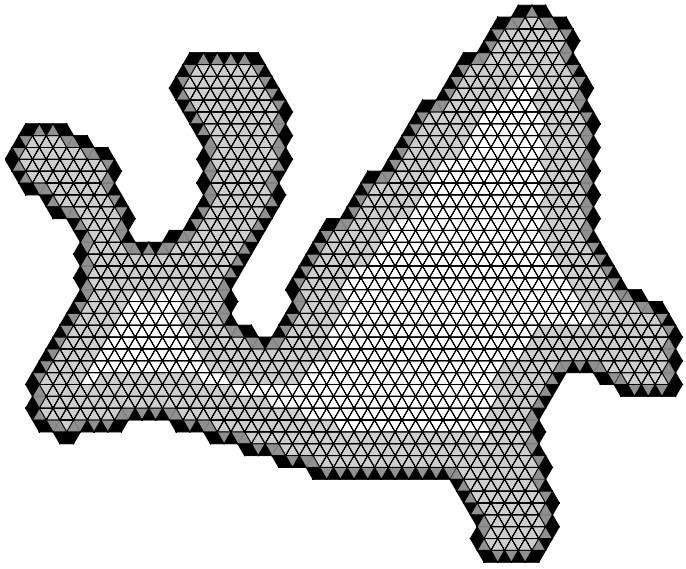

(b) There are 2382 triangles in the collection $\mathcal{T}_h^{0,1,2}$. Of these, 234 triangles belong to $\mathcal{T}_h^2$ (shaded in black), 228 triangles to $\mathcal{T}_h^1$ (shaded in dark gray) and the remaining 1920 triangles to $\mathcal{T}_h^0$. The 756 triangles left unshaded in the figure are the ones that are retained unaltered from the background mesh. The remaining ones have their vertices either snapped onto the boundary or relaxed away from the boundary.

Fig. 2.1: Example illustrating the algorithm in Table 2.1 to mesh an immersed domain by perturbing vertices in a background mesh.

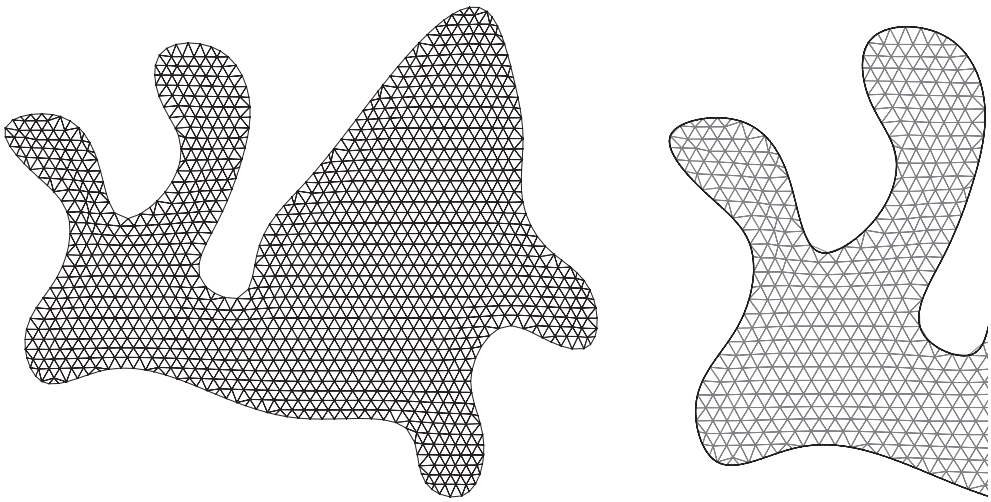

(a) (b)

Fig. 2.2: The conforming mesh determined by the meshing algorithm for the domain and background mesh shown in Fig. 2.1. A closer view is shown in (b).

in this collection are mapped to a conforming mesh for the immersed domain as shown in Fig. 2.2. Of these triangles, 756 remain unaltered from the background mesh. At least one vertex in the remaining triangles is perturbed. Note that with a more refined background mesh, a larger fraction of the triangles in $\mathcal{T}_h^{0,1,2}$ will remain unaltered from the background mesh. For instance, when the background mesh in Fig. 2.1 is refined once by subdivision, 5552 of the 9178 triangles in the resulting conforming mesh remain unaltered (i.e., remain equilateral triangles).

In Table 2.2, we inspect the quality of triangles in the mesh in Fig. 2.2. We use the ratio of the circumradius to the inradius as a metric for the quality of triangles. The best possible value of this ratio is 2, which is attained in equilateral triangles. The table lists the number of triangles in the final mesh with quality in a given range of the metric. The minimum and maximum angles in the mesh were 20.6° and 129.6°. Table 2.2 also reports the quality of the mesh determined by the algorithm upon refining the background mesh in Fig. 2.1a by subdividing each triangle into four self-similar ones. Extreme angles in the resulting mesh for the curved domain were 18.4° and 139.7° respectively.

2.3. Background meshes as *Universal meshes*. An important advantage of admitting nonconforming background meshes is in problems with evolving domains. For then it is possible, at least in principle, to use the same background mesh to triangulate a changing domain. If not for the entire duration of interest, at least for reasonably large changes in the immersed geometry. This motivates the notion of *universal meshes*.

Given a triangulation $\mathcal{T}_h$, let $\mathcal{D}(\mathcal{T}_h)$ denote the class of all domains that can be meshed with the algorithm in Table 2.1 using $\mathcal{T}_h$ as a background mesh. We say that $\mathcal{T}_h$ is a *universal mesh* for domains in $\mathcal{D}(\mathcal{T}_h)$. The utility of this concept lies in the fact that if $\{\Omega_t\}_t$ is the time evolution of a domain $\Omega_0 \in \mathcal{D}(\mathcal{T}_h)$, then often $\{\Omega_t : 0 \le t \le T\} \subset \mathcal{D}(\mathcal{T}_h)$ for a reasonably large time $T > 0$. As the domain develops

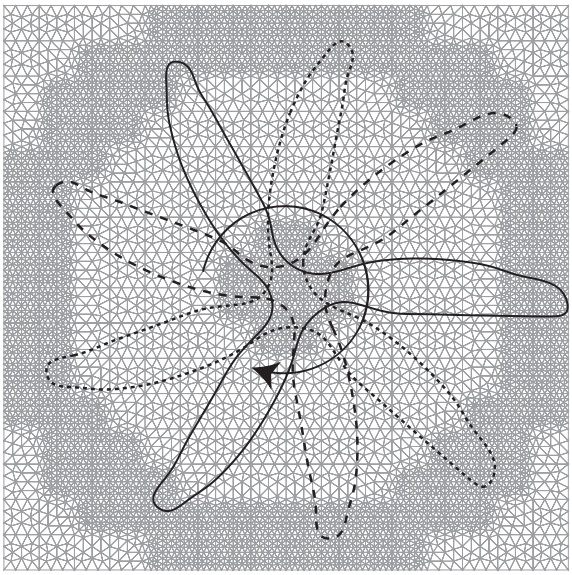

(a)

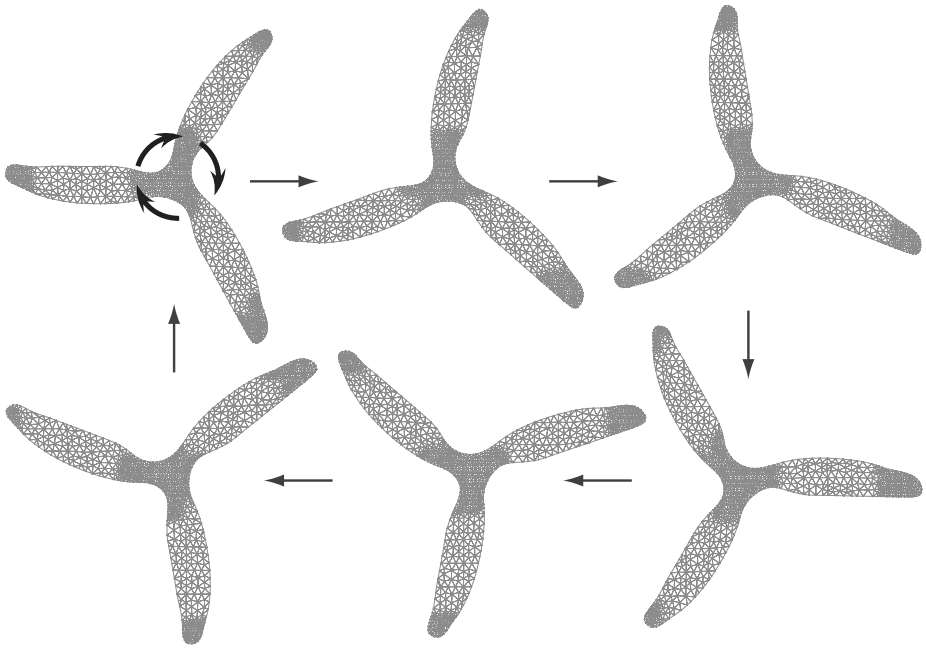

(b)

Fig. 2.3: Example to illustrate the notion of a universal mesh. A three blade propeller rotates about an axis perpendicular to its plane and passing through its center. It is immersed in a refined background mesh of acute angled triangles shown in (a). Using this background mesh in the meshing algorithm in Table 2.1 yields a conforming mesh for each orientation of the propeller; a few are shown in (b). Such a background mesh is hence termed a universal mesh for the domain of the propeller.

Table 2.2: Quality of the mesh determined by the meshing algorithm for the domain in Fig. 2.1a. The metric used for the quality of a triangle is the ratio of its circumradius to the inradius. We only inspect triangles in the final mesh that have been perturbed with respect to the background mesh by the meshing algorithm. The remaining triangles remain equilateral. The column titled 'coarse mesh' lists the number of triangles in the mesh in Fig. 2.2 that have quality in the range specified in the first column. The quality ranges from 2.0 to 5.8. The column titled 'refined mesh' lists corresponding values for the mesh determined using a self-similar refinement of the background mesh shown in Fig. 2.1a. In this case, the quality ranges from 2.0 to 8.8.

Range of metric	coarse mesh	refined mesh
$2.0 - 2.4$	1530	3441
$2.4 - 2.8$	45	75
$2.8 - 3.2$	16	42
$3.2 - 3.6$	9	22
$3.6 - 4.0$	6	11
$4.0 - 4.4$	7	7
$4.4 - 4.8$	5	10
$4.8 - 5.2$	4	3
$5.2 - 5.6$	2	2
$5.6 - 6.0$	2	3
$6.0 - 6.4$	0	2
$6.4 - 6.8$	0	4
> 6.8	0	4

small features or undergoes topological changes, it may no longer belong to $\mathcal{D}(\mathcal{T}_h)$.

We illustrate this idea with the example shown in Fig. 2.3. The domain is a three-blade propeller that rotates about an axis perpendicular to its plane and passing through the center. The background mesh shown in Fig. 2.3a consists of only acute angled triangles. It is refined at the center and along the tips of the blades to resolve the larger curvatures there. This mesh yields a conforming mesh for every orientation of the propeller; a few are shown in Fig. 2.3b. This background mesh is hence a universal mesh for each configuration of the propeller.

An important question in practice is knowing when Ω belongs to $\mathcal{D}(\mathcal{T}_h)$. Precisely characterizing $\mathcal{D}(\mathcal{T}_h)$ is presumably very difficult. Fortunately, it is not essential. Rather, the key step in checking if $\Omega \in \mathcal{D}(\mathcal{T}_h)$ is knowing if $\mathcal{T}_h$ is sufficiently refined in the vicinity of $\partial\Omega$. For this, we will require good, computable and local estimates for the mesh size in order for the meshing algorithm to succeed. As a step in this direction, in [21] we provided upper bounds for the mesh size to guarantee a parameterization of $\partial\Omega$ over positive edges in $\mathcal{T}_h$. An analysis of the meshing algorithm is required to derive a similar bound for the required mesh size of the background mesh.

2.4. Details for the implementation. An implementation of the meshing algorithm is provided in appendix A. We discuss a few details here.

(i) **Identifying vertices in Ω:** The first step in Table 2.1 requires identifying which vertices of $\mathcal{T}_h$ lie in Ω. This is simplest when Ω is represented implicitly, as $\Omega = \{x \in \mathbb{R}^2 : \Psi(x) < 0\}$. For then, a vertex v in $\mathcal{T}_h$ belongs to Ω *iff* $\Psi(v) < 0$. If such a level set function ψ is not known *a priori*, it can be chosen

to be the signed distance function to $\partial\Omega$, $\phi : \mathbb{R}^2 \to \mathbb{R}$ defined as

$$\phi(x) = \begin{cases} -\text{distance}(x, \partial\Omega) & \text{if } x \in \Omega, \\ \text{distance}(x, \partial\Omega) & \text{otherwise.} \end{cases} \tag{2.4}$$

(ii) **Closest point projection:** Mapping vertices of positive edges onto $\partial\Omega$ requires computing the closest point projection to $\partial\Omega$, $\pi : \mathbb{R}^2 \to \partial\Omega$ defined as

$$\pi(x) = \arg\min_{y \in \partial\Omega} \text{distance}(x, y). \tag{2.5}$$

For C^2-regular domains, π is related to the signed distance function ϕ by

$$\pi(x) = x - \phi(x)\nabla\phi(x) \tag{2.6}$$

sufficiently close to $\partial\Omega$, see [21, Theorem 2.2]. Observe that in the meshing algorithm, π needs to be evaluated only over positive edges and that these edges are by definition within a distance h from $\partial\Omega$. Hence relation (2.6) can be used to compute π if $\mathcal{T}_h$ is sufficiently refined. This in turn requires computing ϕ and its derivatives close to the boundary. We refer to appendix A in [23] for a discussion on computing ϕ, π, and their derivatives for parametric and implicit representations of $\partial\Omega$.

(iii) **Relaxing vertices away from $\partial\Omega$:** In step 4 in Table 2.1, vertices in Ω that lie close to $\partial\Omega$ are perturbed away from the boundary. While such perturbations can be realized in numerous ways, we have adopted the map in (2.1). Close to $\partial\Omega$, $\nabla\phi(x)$ equals the unit outward normal to $\partial\Omega$ at $\pi(x)$. Hence $\mathfrak{p}_h(x)$ indeed perturbs vertices *away* from the boundary. By selecting r to be $\mathcal{O}(h)$ in the definition of $\mathfrak{p}_h$, only a small number of vertices near the boundary are perturbed. Such a scaling is also essential in the definition of $\mathfrak{p}_h$ because $\nabla\phi$ may be defined only in a small neighborhood of $\partial\Omega$. In our examples, we pick $\eta \simeq 0.3$ and $r \simeq 3h$. Observe that $\mathfrak{p}_h$ does not move vertices that lie on $\partial\Omega$. Hence steps 3 and 4 in Table 2.1 move exclusive sets of vertices. These two steps can therefore be performed in either order.

(iv) **Tolerances and Round-off:** In identifying which vertices lie in Ω (step 1 in Table 2.1), the effect of tolerances and round-off errors is perhaps unavoidable. As a result, a vertex in Ω may be (mis)identified as lying in Ω^c and vice versa. The effect of tolerances can in fact be understood as introducing small perturbations in the boundary. Incorrectly identifying vertices in Ω will change the collection of positively cut triangles, positive edges and hence the resulting mesh for Ω. However, the resulting mesh will be valid provided conditioning angles remain acute. In particular, if triangles in the vicinity of $\partial\Omega$ are acute angled, the choice of tolerances and the effect of round-off errors is not critical. The resulting mesh may depend on their choice but will be valid nonetheless.

(v) **Background meshes:** For a given curved domain Ω, assumptions (b)–(d) in §2.1 impose restrictions on the background mesh $\mathcal{T}_h$. Since the polygon triangulated by $\mathcal{T}_h$ is quite arbitrary, assumption (b) is easily satisfied. A simple way to satisfy the acute conditioning angle requirement (c) is to ensure that triangles in the vicinity of $\partial\Omega$ are acute angled. An even simpler way is to use a background mesh of all acute angled triangles. For instance, use a mesh of all equilateral triangles as done in the example in Fig. 2.1.

In practice, it is desirable to use an adaptively refined background mesh, depending on the geometric features of the boundary or on the solution being

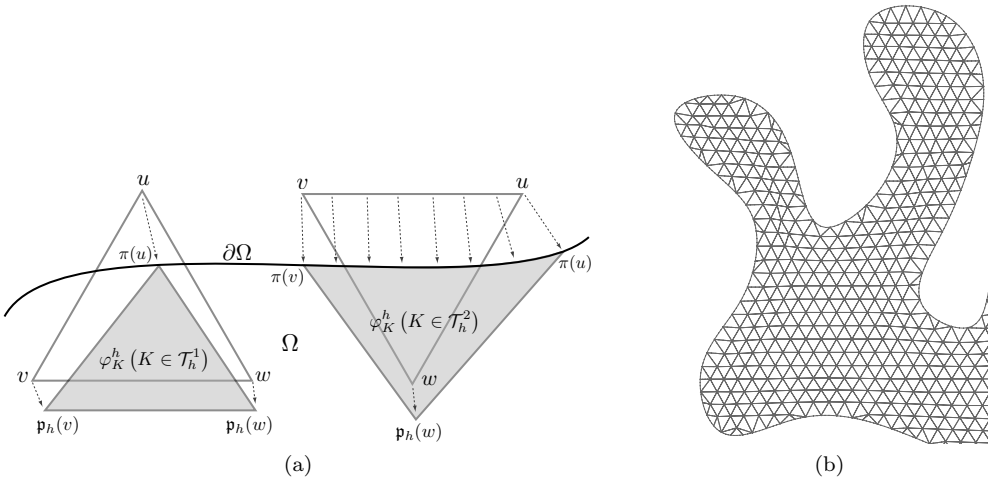

Fig. 3.1: Mappings from triangles in a background mesh to curved triangles that exactly conform to an immersed domain. As shown in (a), the mapping φ_K^h takes positively cut triangles to curved ones that conform to the boundary exactly. This is achieved by ensuring that the restriction of φ_K^h to a positive edge equals the closest point projection π. Triangles with two or more vertices in Ω, i.e., in $\mathcal{T}_h^{0,1}$, are mapped affinely. Figure (b) shows part of the curvilinear mesh obtained by using φ_K^h in the example in Fig. 2.1a.

approximated. A convenient way of doing so is by triangulating adaptively refined quadtrees. Bern et al. [4] provide stencils of acute angled triangles to tile quadtrees. The interior angles of triangles in these stencils lie between 36° and 80°. Therefore, the resulting background meshes automatically satisfy the acute conditioning angle requirement. The background mesh shown in Fig. 2.3a was constructed in this way. We refer to [23] for more examples of background meshes constructed from adaptively refined quadtrees.

3. Exactly conforming curved elements. Curvilinear discretizations provide high-order accurate approximations for curved domains, compared to polygonal ones that results from the meshing algorithm discussed above. Curved finite elements constructed using such discretizations are indispensable for optimal accuracy with high-order interpolations. Curvilinear discretizations broadly fall into two categories. In the first kind, curved triangles conform *exactly* to the domain. In the other, curved triangles approximate the domain sufficiently well and are usually defined via isoparametric mappings. We consider the former here and the latter in §4.

Constructing mappings from straight to curved triangles, even with a conforming mesh, is a delicate task because there are two conflicting requirements. The resulting curved triangle should approximate the domain well. Yet, it should be a sufficiently small perturbation of the straight one if interpolation estimates on the latter are expected to translate into optimal ones over the curved triangle, see [9]. Below we give one such mapping, which generalizes the ones in [13, 28] to the case of nonconforming background meshes.

3.1. Exactly conforming triangles. Defining a curvilinear mesh that conforms exactly to Ω requires only a subtle modification of the meshing algorithm— instead of mapping vertices of positive edges onto $\partial\Omega$, we map positive edges themselves onto $\partial\Omega$. Analogous to the mapping M_K^h in (2.3) that defined the meshing algorithm, we construct a mapping φ_K^h triangle-wise over the collection $\mathcal{T}_h^{0,1,2}$. To this end, consider $K \in \mathcal{T}_h^{0,1,2}$ with vertices $\{u, v, w\}$ ordered such that $\phi(u) \geq \phi(v) \geq \phi(w)$. For $K \in \mathcal{T}_h^{0,1}$, set $\varphi_K^h := M_K^h$. Over positively cut triangles $K \in \mathcal{T}_h^2$, define

$$\begin{aligned}\varphi_K^h(x) := &\frac{1}{2(1-\lambda_u)}\left[\lambda_v \pi\left(\lambda_u\, u + (1-\lambda_u)\, v\right) + \lambda_u\lambda_w\pi(u)\right] \\ &+ \frac{1}{2(1-\lambda_v)}\left[\lambda_u \pi\left((1-\lambda_v)\, u + \lambda_v\, v\right) + \lambda_v\lambda_w\pi(v)\right] \\ &+ \lambda_w \mathfrak{p}_h(w). \end{aligned} \tag{3.1}$$

Note that as in (2.3), the dependence on x in (3.1) is implicit in the barycentric coordinates λ_u, λ_v and λ_w. Unlike M_K^h in (2.3) however, φ_K^h in (3.1) is no longer affine over positively cut triangles. Fig. 3.1a depicts the action of φ_K^h on triangles in $\mathcal{T}_h^{1,2}$. Fig. 3.1b shows part of the curvilinear mesh obtained by using the map φ_K^h in the example in Fig. 2.1. Since φ_K^h differs from M_K^h only over triangles in $\mathcal{T}_h^2$, the curvilinear mesh in Fig. 3.1b differs from the mesh in Fig. 2.2b only over the 234 positively cut triangles.

Let us examine the definition of φ_K^h for $K \in \mathcal{T}_h^2$ in (3.1). By the assumed ordering of vertices, the edge $\overline{uv}$ joining vertices u and v is the positive edge of K. On this edge $\lambda_w = 0$ and $\lambda_u + \lambda_v = 1$. So

$$\varphi_K^h(x \in \overline{uv}) = \frac{1}{2}\pi((1-\lambda_v)\, u + \lambda_v\, v) + \frac{1}{2}\pi(\lambda_u\, u + (1-\lambda_u)\, v) = \pi(x). \tag{3.2}$$

Hence φ_K^h equals the closest point projection over the positive edge $\overline{uv}$. This shows that φ_K^h maps the positive edge onto $\partial\Omega$, as depicted in Fig. 3.1a. On the edge $\overline{uw}$, $\lambda_v = 0$ and $\lambda_u + \lambda_w = 1$. Then (3.1) reduces to

$$\varphi_K^h(x \in \overline{uw}) = \frac{\lambda_u\lambda_w}{2(1-\lambda_u)}\pi(u) + \frac{1}{2}\pi(u) + \lambda_w\mathfrak{p}_h(w) = \lambda_u\, \pi(u) + \lambda_w\mathfrak{p}_h(w), \tag{3.3}$$

which is an affine map. Similarly,

$$\varphi_K^h(x \in \overline{vw}) = \lambda_v\, \pi(v) + \lambda_w\mathfrak{p}_h(w). \tag{3.4}$$

Eqs.(3.2), (3.3) and (3.4) show that φ_K^h can be interpreted as the interpolation to $\overline{K}$, of a map that equals π on the positive edge and is affine on the remaining two. This point of view is also adopted in [13, 17]. For this reason, mappings such as φ_K^h in (3.1) are also commonly termed blending maps and transfinite interpolations.

Remark: We ought to mention an alternate construction for mapping positively cut triangles to curved ones that explicitly uses the meshing algorithm as an intermediate step. In such a construction, the domain Ω is first meshed using the algorithm in §2 and the resulting mesh is then transformed to a curvilinear one that conforms to Ω. More precisely, with $K_S := M_K^h(K)$, the mapping ψ_K^h defined as

$$\psi_K^h := \begin{cases} M_K^h & \text{if } K \in \mathcal{T}_h^{0,1}, \\ \varphi_{K_S}^h \circ M_K^h & \text{if } K \in \mathcal{T}_h^2 \end{cases} \tag{3.5}$$

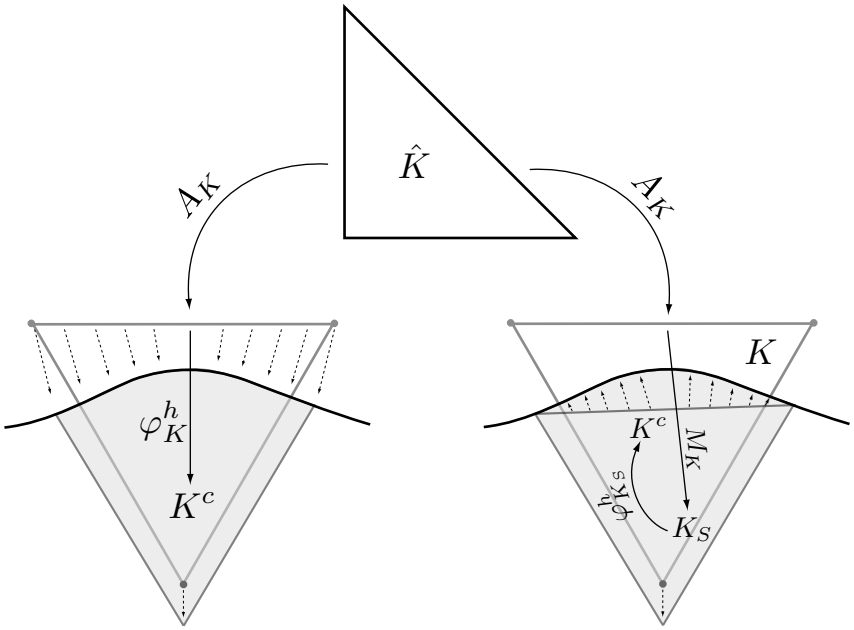

Fig. 3.2: Defining high-order finite elements by constructing mappings from the reference element $\hat{K}$ to the curved element K^c. The figure shows two such mappings. The mapping on the left, namely $\varphi_K^h \circ A_K$, first transforms $\hat{K}$ to the positively cut triangle K in the background mesh and then uses φ_K^h to map K to the curved triangle K^c. The second construction on the right, given by $\varphi_{K_S}^h \circ M_K \circ A_K$ (also equal to $\psi_K^h \circ A_K$), uses the meshing algorithm as an intermediate step. The reference triangle is mapped to K with A_K, then K mapped to the triangle $K_S = M_K(K)$ which is finally transformed to K^c with the map $\varphi_{K_S}^h$.

maps triangles in the collection $\mathcal{T}_h^{0,1,2}$ to a curvilinear mesh that conforms exactly to Ω. Of course, the maps φ_K^h and ψ_K^h differ only for positively cut triangles. For $K \in \mathcal{T}_h^2$, observe

(i) that ψ_K^h first maps K to a conforming triangle K_S and then transforms K_S to a curved triangle, and

(ii) that even though $\varphi_K^h(\overline{K}) = \psi_K^h(\overline{K})$ (as sets in $\mathbb{R}^2$), $\varphi_K^h \neq \psi_K^h$ in general. The two will however be close in a pointwise sense.

The distinction between the φ_K^h and ψ_K^h for positively cut triangles is illustrated in Fig. 3.2.

The conditions in §2.1 suffice for the mappings φ_K^h and ψ_K^h to be well defined and bijective. The mesh size required near the boundary may be smaller for curvilinear discretizations of Ω using φ_K^h or ψ_K^h compared to the mesh size required for the meshing algorithm. This is because we require the Jacobian of these maps to be positive over the entire element.

3.2. High-order finite elements. The mappings φ_K^h and ψ_K^h from straight to curvilinear triangles facilitate a natural construction of curved Lagrange finite elements. The idea behind the construction is illustrated in Fig. 3.2.

3.2.1. Curved finite elements. Introduce the reference triangle $\hat{K} \subset \mathbb{R}^2$ and the finite element triplet $(\hat{K}, \hat{N}^k, \hat{\mathbb{P}}^k)$. As usual, $\hat{\mathbb{P}}^k$ is the set of polynomials over $\hat{K}$ of degree at most k and $\hat{N}^k = \{\hat{N}_a\}_a$ is the set of shape functions that constitute a basis for $\hat{\mathbb{P}}^k$. Associated with $\hat{N}^k$ are the nodes $\{\hat{z}_a\}_a \in \hat{K}$ which are such that $\hat{N}_a(\hat{z}_b) = \delta_{ab}$.

Let $A_K : \hat{K} \to K$ be an affine map from $\hat{K}$ to K. The curved finite element corresponding to $K \in \mathcal{T}_h^{0,1,2}$ derived from $(\hat{K}, \hat{N}^k, \hat{\mathbb{P}}^k)$ is denoted by (K^c, N^k, P^k), where $K^c = \varphi_K^h(K) = \varphi_K^h(A_K(\hat{K}))$ and

$$P^k = \{\hat{p} \circ A_K^{-1} \circ (\varphi_K^h)^{-1} : \hat{p} \in \hat{\mathbb{P}}^k\}. \tag{3.6}$$

In particular, shape functions $\{N_a\}_a$ over K^c are defined by the relation $N_a \circ \varphi_K^h \circ A_K = \hat{N}_a$. Nodes $\{z_a^c\}_a$ in the curved element are located at $z_a^c = \varphi_K^h(A_K(\hat{z}_a))$. Hereafter, the set $\{\hat{z}_a\}$ will be chosen so that finite element functions over Ω are in C^0.

The choice of φ_K^h over ψ_K^h to define the curved element (K^c, N^k, P^k) above was arbitrary; replacing each instance of φ_K^h by ψ_K^h yields a curved element as well. In fact, it may be more convenient to incorporate ψ_K^h into existing finite element codes based on conforming meshes. In the following example as well as the ones in §3.3, we have adopted the curved elements based on the map φ_K^h.

3.2.2. Optimal convergence: numerical example. We demonstrate optimal convergence using the curved finite elements described above with a numerical example. Although the given construction for curved elements is a standard one, the example helps show that the mapping φ_K^h in (3.1) satisfies the conditions in [9] for optimal interpolation estimates over the curved element. We consider the model problem

$$\Delta u = 0 \text{ in } \Omega = \{r = \sqrt{x^2 + y^2} < 1\}, \tag{3.7a}$$

$$u = e^y \sin x \text{ on } \partial\Omega. \tag{3.7b}$$

The solution to (3.7) is the smooth function $u(x, y) = e^y \sin x$. The weak form of (3.7) is to find $u \in H_\partial^1 = \{v \in H^1(\Omega) : v\big|_{\partial\Omega} = e^y \sin x\}$ such that

$$\int_\Omega \nabla u \cdot \nabla v \, d\Omega = 0 \quad \forall v \in H_0^1(\Omega). \tag{3.8}$$

To compute finite element approximations u_h of u, Ω is immersed in background meshes of equilateral triangles. The coarsest background mesh has mesh size $h_0 \simeq 0.27$. Fig. 3.3 shows the convergence of the solution computed with standard Lagrange elements (over $\hat{K}$), as the background mesh is refined (h-refinement). Dirichlet boundary conditions were imposed by interpolating the prescribed function in (3.7b) at the nodes of curved elements lying on the boundary. We used sufficiently accurate quadrature rules to evaluate the stiffness matrix, see §4.1. The convergence rate in the $L^2(\Omega)$-norm is optimal for linear, quadratic, cubic and quartic elements ($k = 1, 2, 3$ and 4 respectively).

Examining $\|u - u_h\|_{L^2(\Omega)}$ in Fig. 3.3 also reveals that for a given background mesh, the error decreases with the element order k. This demonstrates that the curved elements are well suited for p-refinement— progressively accurate solutions can be computed by just increasing the element order while using the *same background mesh*. Moreover, the data in Fig. 3.3 shows that the error is $\mathcal{O}(h^{k+1})$, which is

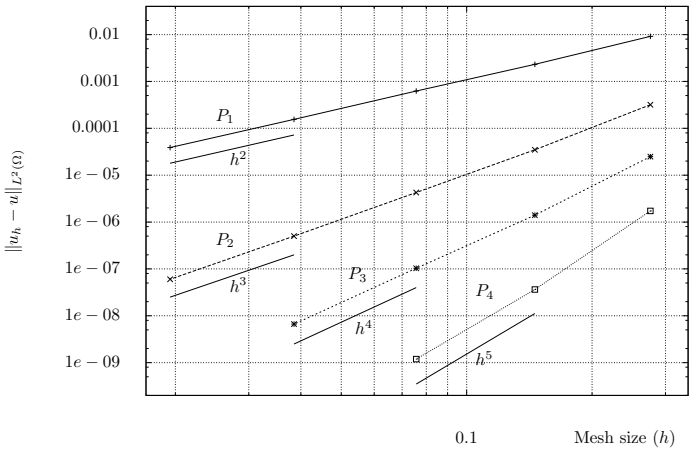

Fig. 3.3: Optimal convergence of the finite element solution u_h, computed using exactly conforming curved elements, to the exact one u of problem (3.7). The plot shows convergence in the $L^2(\Omega)$-norm as the background mesh is refined. The rate of convergence is optimal for linear, quadratic, cubic and quartic elements.

optimal in the element order k for each given (sufficiently small) mesh size h of the background mesh. Such optimal convergence rates would also be obtained with the isoparametric curved elements described subsequently in §4.

3.3. Applications: Evolving fluid domains. Next, we present two applications using the curved elements described above. In both examples, a fixed background mesh serves as the universal mesh for an evolving fluid domain.

3.3.1. Flow with a rotating component. We consider the example mentioned in §1, of a propeller mixing fluid in a closed container. The problem setup is the same one illustrated in Fig. 2.3, although the container B is larger. The propeller P is assumed to be rigid and impermeable. It rotates with constant angular velocity ω about an axis passing through its center and perpendicular to its plane. The fluid in the container is incompressible and has viscosity μ. Its kinematics is governed by the familiar equations for Stokes flow,

$$\mu \operatorname{div}(\nabla \mathbf{u}_t) = \nabla p_t, \tag{3.9a}$$

$$\operatorname{div}(\mathbf{u}_t) = 0, \tag{3.9b}$$

relating the flow velocity $\mathbf{u}_t$ and pressure p_t at time t. No-slip boundary conditions along the walls of the container and the boundary of the propeller imply

$$\mathbf{u}_t = \begin{cases} 0 & \text{on } \partial B, \\ r\omega\, \mathbf{e}_\theta & \text{on } \partial P_t, \end{cases} \tag{3.10}$$

where P_t is the configuration of the propeller at time t and $\{\mathbf{e}_r, \mathbf{e}_\theta\}$ is a canonical polar basis for a polar coordinate system with origin at the center of P. Since (3.9) and (3.10) determine the pressure only up to a constant, p_t is assigned to be zero at one point in the flow domain, i.e., we set $p_t = 0$ at $x_0 \in B \setminus P_t$.

A triangulation of B, similar to the one shown in Fig. 2.3a, serves as the universal mesh for the fluid domain $B \setminus P_t$. The mesh is refined further near the tips of the blades to resolve features of the flow there. We adopt (curved) Taylor-Hood elements for the finite element solution of (3.9), i.e., the element (K^c, N^2, P^2) for the velocity $\mathbf{u}_t$ and (K^c, N^1, P^1) for the pressure p_t. See [11] for a discussion on the Taylor-Hood element and for the weak form of this problem, which we have omitted here. Dirichlet boundary conditions are imposed by interpolating (3.10) at the nodes lying

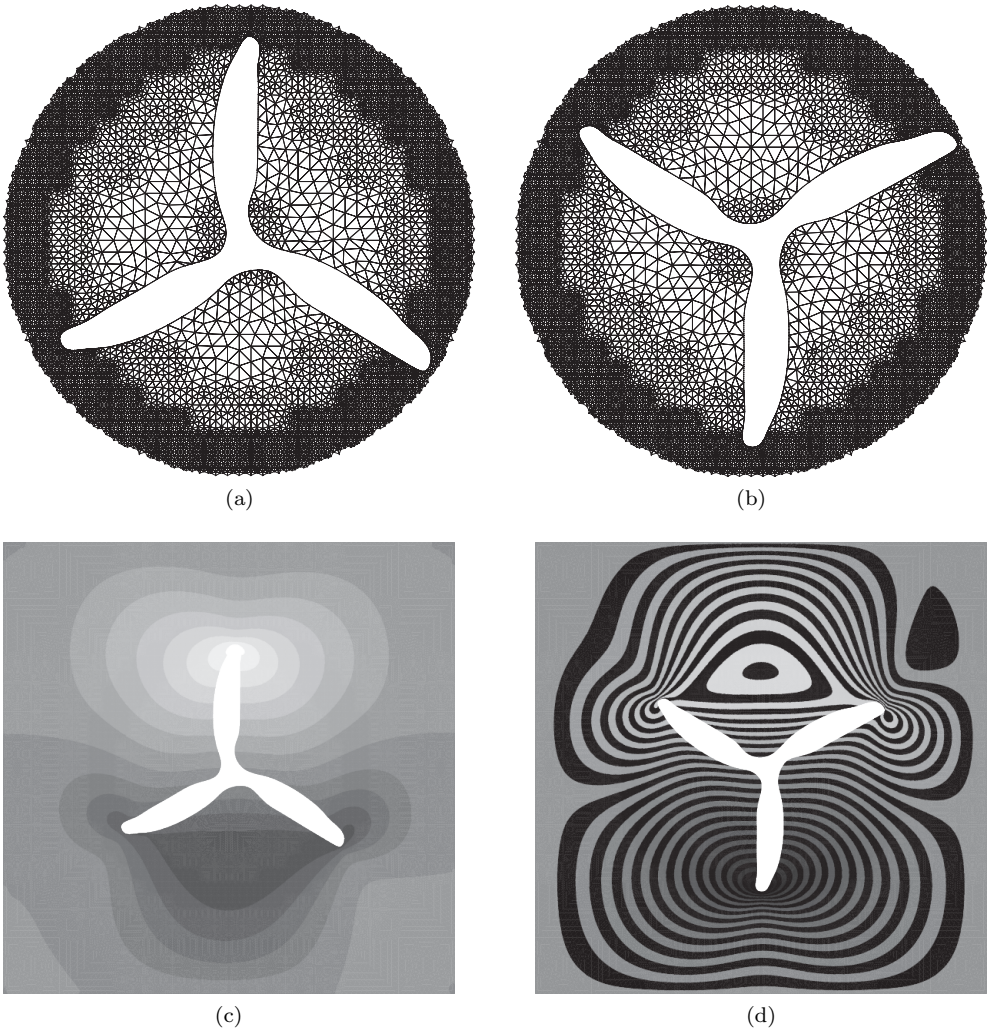

Fig. 3.4: Simulating Stokes flow driven by a rotating propeller in a closed container. At each instant, the same background mesh is used to determine a curvilinear mesh that conforms exactly to the fluid domain. Figures (a) and (b) show the elements close to the propeller in the resulting mesh at two distinct times. Contours of the horizontal component of the flow velocity at these times are shown in figures (c) and (d). To highlight the flow pattern, the contours are shown with zebra shading in (d).

on the boundary. Figs. 3.4a and 3.4b show the curvilinear mesh conforming to the fluid domain at three different time instants. Since the mesh is quite refined, only the elements near the propeller are shown. Corresponding to these orientations of the propeller, Figs. 3.4c and 3.4d show contours of the horizontal component of the velocity computed with $\mu = 0.01$ and $\omega = 2$.

3.3.2. Flow interaction with a rigid disc. In the second example, we consider the interaction between a fluid and a rigid solid. The problem is to determine the

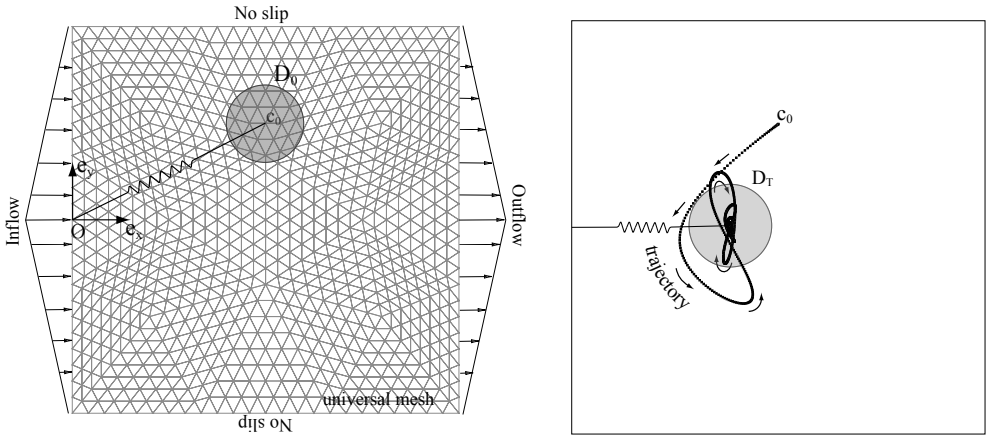

(a) (b)

Fig. 3.5: Figure (a) shows the initial setup for the problem of a rigid disc D interacting with an incompressible fluid. The disc is attached to the origin by a linear spring. Inflow and outflow boundary conditions for the flow through the channel B are indicated. A simple, unstructured mesh of B serves as the universal mesh for the fluid for the entire duration of the simulation. Figure (b) shows the trajectory computed for the disc as it moves from its initial position to an (approximate) equilibrium position.

trajectory of a rigid disc D of radius R and mass m immersed in an incompressible, viscous fluid flowing through a square shaped channel B of side L. The disc is attached to the origin O located at the mid-point of the left end of the channel by a linear spring with spring constant k and equilibrium length ℓ_0. The problem setup is shown in Fig. 3.5a.

We assume that the kinematics of the fluid is governed by the equations for Stokes flow given in (3.9), retaining the notation introduced there. In a Cartesian coordinate system centered at O, inflow and outflow boundary conditions are prescribed at the two ends of the flow channel as

$$\mathbf{u}_t = (L - 2|y|)\mathbf{e}_x \quad \text{if } x = 0, L. \tag{3.11}$$

Denote the position of the center of the disc at time t by $\mathbf{c}(t)$ and the disc centered at $\mathbf{c}(t)$ by D_t. No-slip boundary conditions along the horizontal walls of the channel and along the boundary of the disc imply

$$\mathbf{u}_t = \begin{cases} 0 & \text{if } |y| = L/2, \\ \dot{\mathbf{c}}(t) & \text{on } \partial D_t. \end{cases} \tag{3.12}$$

Force balance for the disc is given by

$$m\,\ddot{\mathbf{c}} = k\left(1 - \frac{\ell_0}{|\mathbf{c}|}\right)\mathbf{c} + \int_{\partial D_t} \boldsymbol{\sigma}_f \cdot \mathbf{n}_t \, ds, \tag{3.13}$$

where $\mathbf{n}_t$ is the unit outward normal to ∂D_t and the stress $\boldsymbol{\sigma}_f$ in the fluid is computed as

$$\boldsymbol{\sigma}_f = -p_t\,\mathbb{I} + \mu\left(\nabla\mathbf{u}_t + \nabla\mathbf{u}_t^T\right).$$

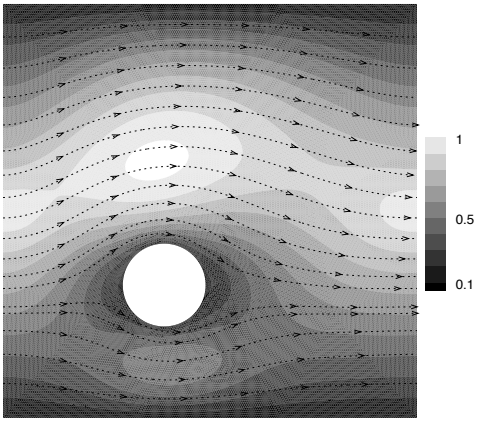

Fig. 3.6: Contours of the horizontal component of the flow velocity at a non-equilibrium position of the disc in the problem described in Fig. 3.5a.

Balance equations (3.9), (3.13), boundary conditions (3.11), (3.12), initial conditions $\mathbf{c}(0) = \mathbf{c}_0$, $\dot{\mathbf{c}}(0) = 0$, and $p_t(x_0 \in B \setminus D_t) = 0$ together constitute a coupled system of equations for the unknowns $(\mathbf{u}_t, p_t)$ and $\mathbf{c}(t)$. We use (curved) Taylor-Hood elements for the flow solution as before and adopt a staggered time integration scheme. At each time instant t_n, given the center of the disc $\mathbf{c}_n$ and its velocity $\dot{\mathbf{c}}_n$, we define curvilinear elements for the flow variables over $B \setminus D_t$. We then compute the flow solution $(\mathbf{u}_n^h, p_n^h)$ at this time. The net force on the disc is evaluated using (3.13). Using central differences, we update the position and velocity of the disc to the next instant t_{n+1} and repeat the process.

The background mesh shown in Fig. 3.5a serves as a universal mesh for the flow domain $B \setminus D_t$. Fig. 3.5b shows the trajectory determined for the disc and its final configuration computed with parameters $L = 1$ for the container, $\mu = 0.01$ for the fluid, $R = L/10, m = 1$ for the disc, $k = 1, \ell_0 = L/4$ for the spring, $\mathbf{c}_0 = (0, L/4)$ for the initial position of the disc and a time step $\Delta t = 0.05$. At an intermediate position of the disc, contours of the horizontal component of the flow velocity along with a few stream lines are shown in Fig. 3.6. The trajectory of the disc plotted in Fig. 3.5b shows that the disc eventually settles to an equilibrium position balancing the forces exerted by the fluid and the spring.

We conclude this section mentioning that there are various numerical methods in the literature for such problems over changing flow domains, see for instance [3, 10, 24, 27].

4. Isoparametric mappings. Isoparametric mappings provide a convenient way of approximating curved domains with a desired accuracy. A systematic definition of these polynomial mappings results naturally from interpolating $\varphi_K^h \circ A_K$ or $\psi_K^h \circ A_K$ at selected points. Since $\varphi_K^h \circ A_K$ and $\psi_K^h \circ A_K$ are affine for $K \in \mathcal{T}_h^{0,1}$, these maps differ from their interpolants only for positively cut triangles ($\mathcal{T}_h^2$). With an isoparametric map, positive edges are mapped to curved ones that interpolate the boundary at a few points. Fig. 4.1 depicts this for the case of a quadratic element.

Following the notation in §3.2, introduce the interpolation operator $\hat{\Pi}^k : f \in [C^0(\hat{K})]^2 \to \sum_a f(\hat{z}_a)\hat{N}_a \in \mathbb{P}^k$. The isoparametric map over $\hat{K}$ corresponding to triangle $K \in \mathcal{T}_h^{0,1,2}$ is defined as

$$I_K^h := \hat{\Pi}^k(\varphi_K^h \circ A_K) = \sum_a \varphi_K^h(z_a) N_a. \tag{4.1}$$

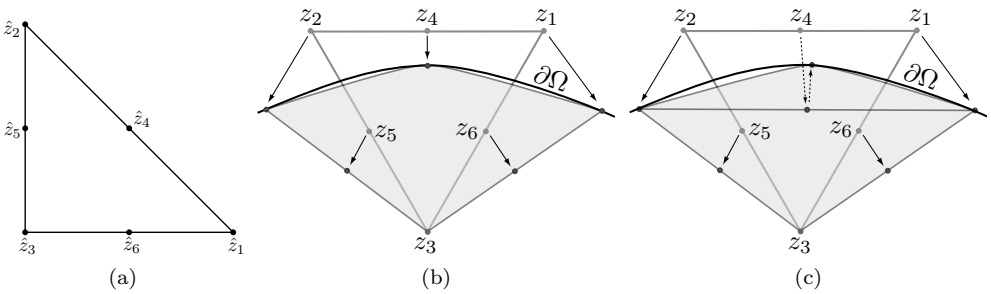

Fig. 4.1: Isoparametric mappings for positively cut triangles in the background mesh. The reference quadratic element is shown in (a). The isoparametric maps constructed by interpolating the mappings $\varphi_K^h \circ A_K$ and $\psi_K^h \circ A_K$ are shown in (a) and (b). The curved boundary of the element interpolates the boundary at the points where the nodes $\hat{z}_1, \hat{z}_2$ and $\hat{z}_4$ are mapped. Notice that the mid-side node $\hat{z}_4$ is generally mapped differently by φ_K^h and ψ_K^h.

Using ψ_K^h instead of φ_K^h yields a different isoparametric map

$$J_K^h := \hat{\Pi}^k(\psi_K^h \circ A_K) = \sum_a \varphi_{K_S}^h(M_K(z_a))N_a. \tag{4.2}$$

As illustrated in Fig. 4.1 for the case of a quadratic element, $I_K^h \neq J_K^h$ in general. In the figure for instance, $I_K^h(\hat{z}_4) = \pi((z_1 + z_2)/2)$ while $J_K^h(\hat{z}_4) = \pi((\pi(z_1) + \pi(z_2))/2)$. Nonetheless, the two maps will be close for small values of h. Curved finite elements using these isoparametric maps are constructed just as in §3.2 by replacing maps φ_K^h or ψ_K^h by their respective interpolants.

Compared to the exactly conforming curved elements, isoparametric elements require fewer evaluations of π in general. Notice from (3.1) that once π is computed at the vertices of the positive edge, defining I_K^h (or J_K^h) requires evaluating π at most twice *per node* in the element. In contrast, computing φ_K^h (or ψ_K^h) at *each quadrature point* requires two new evaluations in the conforming curved element. Furthermore, computing derivatives of shape functions in the isoparametric element does not require computing derivatives of π. However in the conforming curved element, shape function derivatives depend on $\nabla\varphi_K^h$ (or $\nabla\psi_K^h$) which in turn depend on $\nabla\pi$.

4.1. Quadrature for curved elements. For optimal convergence and accuracy of numerical solutions computed using curved elements, we naturally require sufficiently accurate quadrature rules for integration over curvilinear domains. Following standard practice, these quadrature rules need only be defined over the reference triangle, since integrals over a curved element K^c can be performed over $\hat{K}$ using the correspondence provided by the mappings I_K^h (or J_K^h). We adopted for curved elements the same quadrature rules needed for straight elements, as explained in [8]. For example, a quadrature rule that exactly integrates quadratic polynomials over the reference element suffices for isoparametric quadratic elements, so three quadrature points were adopted for those. We have used such integration rules in all of our examples, including the ones with exactly conforming curved elements. These examples suggest that the quadrature rules for straight elements are also enough to obtain optimal convergence rates with exactly curved elements. We also note that

different rules can be used for integrating each term in the weak form of a problem, for instance the mass and stiffness matrices, and the force vector.

4.2. Circular plate in bending. We consider the problem of a thick, circular, elastic plate bending under the action of a uniform external load. As pointed out in [2], this problem highlights the importance of representing curved boundaries accurately. We present this example to emphasize the distinction between representing a curved boundary exactly using the elements in §3 and approximating it with isoparametric elements as defined above. Consider a Cartesian coordinate system (x, y, z) with basis $\{\mathbf{e}_x, \mathbf{e}_y, \mathbf{e}_z\}$. The domain of the problem is the set $\Omega \times (-t/2, t/2)$, where Ω is a circle of radius $R = 3.142$ centered at the origin and contained in the plane of $\mathbf{e}_x, \mathbf{e}_y$, and t is the thickness along $\mathbf{e}_z$. We assume that the displacement field $\mathbf{u}$ of the plate is of the form

$$\mathbf{u}(x, y, z) = -z\,(\vartheta_x(x, y)\mathbf{e}_x + \vartheta_y(x, y)\mathbf{e}_y) + w(x, y)\mathbf{e}_z, \tag{4.3}$$

which corresponds to the Reissner-Mindlin model for a thick plate in bending, see [2, 7]. In (4.3), w is the transverse displacement of points in the mid-plane Ω while ϑ_x and ϑ_y represent the infinitesimal rotations of fibers normal to the mid-plane about the axes $\mathbf{e}_y$ and $\mathbf{e}_x$, respectively. We consider a "soft-simple support" for the plate, which implies the boundary conditions

$$\left.\begin{aligned} w &= 0 \\ \boldsymbol{\vartheta} \cdot \mathbf{t} &= 0 \end{aligned}\right\} \text{ on } \partial\Omega \tag{4.4}$$

where $\mathbf{t}$ is the unit tangent to $\partial\Omega$ and $\boldsymbol{\vartheta} = (\vartheta_x, \vartheta_y)$. The plate is loaded by a constant force $2p$ normal to its top face $\Omega \times \{t/2\}$. The elasticity problem is then to find

$$\begin{aligned} \mathbf{u} &\in \left\{-z\,\boldsymbol{\vartheta} + w\,\mathbf{e}_z \,:\, \boldsymbol{\vartheta} \in \mathbf{H}^1_t, w \in H^1_0(\Omega)\right\}, \\ \text{where } \ \mathbf{H}^1_t(\Omega) &:= \{\boldsymbol{\vartheta} \in [H^1(\Omega)]^2 \,:\, \boldsymbol{\vartheta} \cdot \mathbf{t} = 0 \text{ on } \partial\Omega\}, \end{aligned}$$

which minimizes the strain energy functional

$$I[\mathbf{u}] = \frac{1}{2}\int_{\Omega\times(-t/2,t/2)} \left\{\lambda[\mathrm{tr}(\boldsymbol{\varepsilon}(\mathbf{u}))]^2 + 2\mu\,\boldsymbol{\varepsilon}(\mathbf{u}) : \boldsymbol{\varepsilon}(\mathbf{u})\right\} - \int_\Omega p\,w, \tag{4.5}$$

where λ, μ are material parameters called Lamé constants and $\varepsilon(\mathbf{u}) = (\nabla\mathbf{u} + \nabla\mathbf{u}^T)/2$ is the usual infinitesimal strain tensor. Introducing assumption (4.3) in (4.5) and integrating along the thickness reduces (4.5) to a problem over Ω: find $(\boldsymbol{\vartheta}, w) \in \mathbf{H}^1_t(\Omega) \times H^1_0(\Omega)$ that minimizes the functional

$$\begin{aligned} F[(\boldsymbol{\vartheta}, w)] = \frac{1}{2}\int_\Omega \left\{\lambda\left[\mathrm{tr}\left(\boldsymbol{\varepsilon}(\boldsymbol{\vartheta})\right)\right]^2 + 2\mu\,\boldsymbol{\varepsilon}(\boldsymbol{\vartheta}) : \boldsymbol{\varepsilon}(\boldsymbol{\vartheta})\right\} \\ + \frac{6\mu}{t^2}\int_\Omega \|\boldsymbol{\vartheta} - \nabla w\|^2 - \frac{12}{t^3}\int_\Omega pw. \end{aligned} \tag{4.6}$$

We compare the transverse displacements at the center of the plate as the background mesh for Ω is refined, while using curved quadratic elements. We pick $\lambda = \mu = 1, t = R/4$ for the plate and $p = 1\times10^{-3}$ for the loading. We take as a reference value $w_0 = 5.3407075\times10^{-2}$, computed with exactly conforming curved quartic elements (see §3.2) and a refined background mesh of equilateral triangles. Table

Table 4.1: Transverse displacements at the center of the circular plate Ω computed with curved quadratic elements. The reference value is $w_0 = 5.3407075\times10^{-2}$. The columns titled 'conforming' and 'isoparametric' list the values computed with exactly conforming elements and isoparametric elements, respectively. The column 'modified isoparametric' contains the values computed with isoparametric elements but while imposing the constraint $\boldsymbol{\vartheta}\cdot\mathbf{t}=0$ using one of the two possible tangents $\mathbf{t}$ at vertices on the curved edges of the element. The coarsest mesh size of the background mesh is $h_0 \simeq 0.28R$.

mesh size	conforming ($\times10^{-2}$)	isoparametric ($\times10^{-2}$)	modified isoparametric ($\times10^{-2}$)
h_0	5.3370662	2.2343001	5.3383666
$h_0/2$	5.3401468	1.9557577	5.3400195
$h_0/4$	5.3406606	1.8019916	5.3406438
$h_0/8$	5.3407108	1.6864489	5.3407156

4.1 lists the displacements computed with exactly conforming quadratic elements and with isoparametric quadratic elements.

From the table, we see that the displacements computed with the conforming elements converge to w_0. But somewhat surprisingly, those computed with quadratic isoparametric elements fail to even come close to w_0. This is a consequence of enforcing the constraint on rotations in (4.4) on the approximate curved boundary realized with isoparametric elements. The unit tangent to this boundary fails to be continuous at vertices that lie on it. Consequently, rotations equal zero at each vertex on the boundary. With exactly conforming curved elements, $\partial\Omega$ is represented exactly and this issue is avoided.

The above discussion shows that the constraint in (4.4) needs to be enforced differently. For instance, we could select one of the tangents at each vertex on the approximate boundary to enforce the constraint $\boldsymbol{\vartheta}\cdot\mathbf{t}=0$. The displacements computed with quadratic isoparametric elements by enforcing the constraint in this way are listed under the column title 'modified isoparametric' in Table 4.1. These values are clearly more accurate and converge to w_0.

Remark: We have used the same finite element spaces for both transverse displacements (w) and rotations (ϑ_x, ϑ_y) in the above calculations. It is well known that for thin plates ($t \ll R$), such a choice of spaces in the Reissner-Mindlin model results in locking, cf. [7]. To avoid adopting very small mesh sizes for accuracy, we deliberately chose a large thickness $t = R/4$ in the example.

5. Rationale behind algorithm. The meshing algorithm determines a conforming mesh for Ω by perturbing vertices in the triangulation $\mathcal{T}_h^{0,1,2}$. Here we briefly discuss the rationale behind the vertex adjustments we perform— why we perturb vertices in a particular way and when such perturbations are possible.

Mapping vertices to their closest point on $\partial\Omega$: Each vertex of a positive edge is mapped to its closest point on the boundary. This step transforms $\mathcal{T}_h^{0,1,2}$ into a conforming mesh for Ω. The reason is an intuitive one. As we discuss below, the only vertices in $\mathcal{T}_h^{0,1,2}$ that lie outside Ω are the vertices of positive edges. Moreover, the collection of positive edges are the boundary edges of $\mathcal{T}_h^{0,1,2}$ because each of these edges belongs to just one positively cut triangle. By snapping vertices of positive edges onto $\partial\Omega$, every vertex in the resulting mesh belongs to $\overline{\Omega}$ and the boundary edges in the final mesh interpolate $\partial\Omega$.

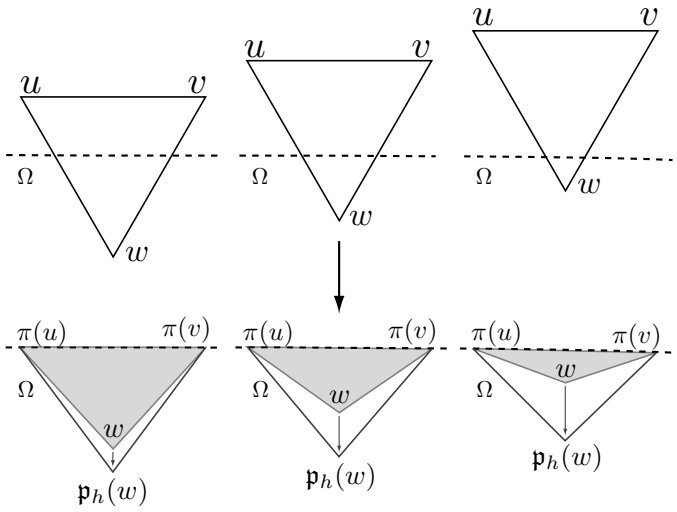

Fig. 5.1: Vertices in Ω near its boundary need to be relaxed away from the boundary in the meshing algorithm to ensure good quality triangles. The figure shows a positively cut triangle with vertices $\{u, v, w\}$ and positive edge $\overline{uv}$. Step 3 in Table 2.1 moves vertices u and v to $\pi(u)$ and $\pi(v)$ respectively. The quality of the resulting triangle with vertices $\{\pi(u), \pi(v), w\}$(shaded in gray) depends on the distance of w from $\partial\Omega$. The three cases in the figure show that the closer w is to $\partial\Omega$, the poorer the quality of the shaded triangle. Perturbing w away from $\partial\Omega$ alleviates this.

A small mesh size near $\partial\Omega$ is essential for this perturbation step. For otherwise, π may be multi-valued at vertices of positive edges. A small mesh size is also required to know that positive edges are boundary edges of $\mathcal{T}_h^{0,1,2}$. If the mesh size is too large, it is possible for two positively cut triangles to share a common positive edge. The acute conditioning angle assumption in §2.1 is critical as well— it ensures that both vertices of a positive edge never map to the same point in $\partial\Omega$ hence preventing positively cut triangles from being mapped to degenerate ones. In fact, using the assumptions in §2.1, we proved in [21] that the restriction of π to the collection of positive edges is a homeomorphism onto $\partial\Omega$ with Jacobian bounded away from zero. Hence we know that moving vertices of positive edges onto the boundary does not yield a tangled mesh. The bound for the Jacobian also implies that positive edges are mapped to interpolating edges whose lengths are neither too small nor too large. We refer to [21, 23] for a detailed discussion on the sufficiency of the assumptions in §2.1 to show that $\partial\Omega$ is parameterized over the collection of positive edges. There we also mention a way of relaxing the acute conditioning angle assumption.

Relaxing vertices away from $\partial\Omega$: Next we explain using an example why it is necessary to relax vertices away from the boundary (step 4 in Table 2.1). Consider a positively cut triangle K with vertices $\{u, v, w\}$ and positive edge $\overline{uv}$ as shown in Fig. 5.1. By snapping vertices u and v onto $\partial\Omega$ in step 3 in the algorithm, K is mapped to a triangle $\tilde{K}$ with vertices $\{\pi(u), \pi(v), w\}$ (shaded in gray in the figure). We know from the above discussion that the length of the edge $\overline{\pi(u)\pi(v)}$ cannot be too small. However, lengths edges $\overline{\pi(u)w}$ and $\overline{\pi(v)w}$ can be arbitrarily small. As depicted in the figure, the closer w is to $\partial\Omega$, the poorer the quality of triangle $\tilde{K}$. To alleviate this,

we move vertex w away from $\partial\Omega$ by a small distance. In turn, to accommodate such perturbations, vertices in a small neighborhood of $\partial\Omega$ are relaxed away from it.

In the map $\mathfrak{p}_h$ used to relax vertices in the algorithm, the parameter r determines the neighborhood of $\partial\Omega$ in which vertices are perturbed. Since we pick r to be a few multiples of the mesh size near $\partial\Omega$, $\mathfrak{p}_h$ is only a local perturbation near $\partial\Omega$. To prevent this step from inducing overlapping or poorly shaped triangles, a small-enough mesh size is also needed. For example, π needs to be well defined in the r-neighborhood of $\partial\Omega$, so that $\mathfrak{p}_h$ is well defined as well over the vertices that are relaxed. Although a detailed analysis is still needed, this step does not appear to pose more stringent requirements on the mesh size that those posed by φ_K^h or Ψ_K^h.

6. Concluding remarks. The meshing algorithm, the mappings to curvilinear triangles used in constructing high-order curved finite elements, and the idea of universal meshes are useful tools for an important class of computationally challenging problems. By employing them in problems with evolving fluid domains while using a single background mesh, we demonstrated the algorithmic advantages they offer. We envision their application to more demanding problems ranging from dynamic crack propagation to phase transformations.

For these tools to also be useful in realistic engineering applications, important questions remain. A significant one is knowing what is a sufficiently small mesh size for the background mesh. A computable estimate is valuable because it can help determine if and when a background(universal) mesh needs to be changed during the course of simulating an evolving domain. The mesh size estimates in [21] for parameterizing the immersed boundary will be useful in determining such bounds.

A second challenge is summarized by the fact that while we can mesh extremely complex smooth domains using a simple background mesh, we have not specified how to mesh a square. This is essentially a consequence of choosing the closest point projection to parameterize the boundary. Whether domains with corners, cracks, and interfaces can be handled without introducing additional restrictions on the background mesh remains to be seen. An important step towards meshing such domains is parameterizing immersed curves with end points and corners. We have shown how to do this in [23].

We think the ideas introduced here can be extended to meshing three dimensional domains immersed in background meshes of tetrahedral meshes. An analysis will reveal the necessary requirements on the background mesh.

Finally, we mention that maintaining the regularity of evolving boundaries has been a recurring challenge in numerical methods for moving boundary problems. It requires careful choices for representing the domain and for schemes to advance the boundary. The literature on these topics is growing and will continue to benefit from each new contribution.

REFERENCES

[1] P. Angot, C.H. Bruneau, and P. Fabrie, *A penalization method to take into account obstacles in incompressible viscous flows*, Numerische Mathematik, 81 (1999), pp. 497–520.

[2] I. Babuška and J. Pitkäranta, *The plate paradox for hard and soft simple support*, SIAM Journal on Mathematical Analysis, 21 (1990), p. 551.

[3] Y. Bazilevs, V.M. Calo, T.J.R. Hughes, and Y. Zhang, *Isogeometric fluid-structure interaction: theory, algorithms, and computations*, Computational Mechanics, 43 (2008), pp. 3–37.

[4] M. Bern, D. Eppstein, and J. Gilbert, *Provably good mesh generation*, Journal of Computer and System Sciences, 48 (1994), pp. 384–409.

[5] C. Börgers, *A triangulation algorithm for fast elliptic solvers based on domain imbedding*, SIAM Journal on Numerical Analysis, (1990), pp. 1187–1196.
[6] E. Burman and P. Hansbo, *Fictitious domain finite element methods using cut elements: I. a stabilized lagrange multiplier method*, Computer Methods in Applied Mechanics and Engineering, 199 (2010), pp. 2680–2686.
[7] D. Chapelle and K.J. Bathe, *The finite element analysis of shells: fundamentals*, Springer Verlag, 2003.
[8] P.G. Ciarlet, *The finite element method for elliptic problems*, vol. 4, North Holland, 1978.
[9] P.G. Ciarlet and P.A. Raviart, *Interpolation theory over curved elements, with applications to finite element methods*, Computer Methods in Applied Mechanics and Engineering, 1 (1972), pp. 217–249.
[10] J. Donea, A. Huerta, J.P. Ponthot, and A. Rodríguez-Ferran, *Arbitrary Lagrangian–Eulerian methods*, Encyclopedia of Computational Mechanics, (2004).
[11] V. Girault and P. Raviart, *Finite element methods for Navier-Stokes equations: Theory and Algorithms*, vol. 5 of Springer Series in Computational Mathematics, Springer-Verlag, Berlin and New York, 1986.
[12] M. Gonzalez and M. Goldschmit, *Inverse geometry heat transfer problem based on a radial basis functions geometry representation*, International journal for numerical methods in engineering, 65 (2006), pp. 1243–1268.
[13] W.J. Gordon and C.A. Hall, *Transfinite element methods: blending-function interpolation over arbitrary curved element domains*, Numerische Mathematik, 21 (1973), pp. 109–129.
[14] A. Hansbo and P. Hansbo, *An unfitted finite element method, based on nitsche's method, for elliptic interface problems*, Computer methods in applied mechanics and engineering, 191 (2002), pp. 5537–5552.
[15] M. Lenoir, *Optimal isoparametric finite elements and error estimates for domains involving curved boundaries*, SIAM Journal on Numerical Analysis, (1986), pp. 562–580.
[16] A.J. Lew and G.C. Buscaglia, *A discontinuous-Galerkin-based immersed boundary method*, International Journal for Numerical Methods in Engineering, 76 (2008), pp. 427–454.
[17] L. Mansfield, *Approximation of the boundary in the finite element solution of fourth order problems*, SIAM Journal on Numerical Analysis, (1978), pp. 568–579.
[18] M. Moumnassi, S. Belouettar, E. Bechet, S. Bordas, D. Quoirin, and M. Potier-Ferry, *Finite element analysis on implicitly defined domains: An accurate representation based on arbitrary parametric surfaces*, Computer methods in applied mechanics and engineering, 200 (2011), pp. 774–796.
[19] S. Osher and R.P. Fedkiw, *Level set methods and dynamic implicit surfaces*, vol. 153, Springer Verlag, 2003.
[20] C.S. Peskin, *The immersed boundary method*, Acta Numerica, 11 (2002), pp. 479–517.
[21] R. Rangarajan and A.J. Lew, *Analysis of a method to parameterize planar curves immersed in triangulations*, ArXiv e-prints, (2011).
[22] R. Rangarajan, A.J. Lew, and G.C. Buscaglia, *A discontinuous-Galerkin-based immersed boundary method with non-homogeneous boundary conditions and its application to elasticity*, Computer Methods in Applied Mechanics and Engineering, 198 (2009), pp. 1513–1534.
[23] Ramsharan Rangarajan and Adrian J. Lew, *Parameterization of planar curves immersed in triangulations with application to finite elements*, International Journal for Numerical Methods in Engineering, 88 (2011), pp. 556–585.
[24] P. Saksono, W. Dettmer, and D. Perić, *An adaptive remeshing strategy for flows with moving boundaries and fluid–structure interaction*, International Journal for Numerical Methods in Engineering, 71 (2007), pp. 1009–1050.
[25] R. Sanches, P. Bornemann, and F. Cirak, *Immersed b-spline (i-spline) finite element method for geometrically complex domains*, Computer Methods in Applied Mechanics and Engineering, (2011).
[26] R. Scott, *Finite element techniques for curved boundaries*, PhD thesis, Massachusetts Institute of Technology, Cambridge, 1973.
[27] G. Wagner, N. Moës, W. Liu, and T. Belytschko, *The extended finite element method for rigid particles in stokes flow*, International Journal for Numerical Methods in Engineering, 51 (2001), pp. 293–313.
[28] M. Zlámal, *Curved elements in the finite element method. I*, SIAM Journal on Numerical Analysis, (1973), pp. 229–240.

Appendix A. Implementation for the meshing algorithm. We provide a simple implementation of the meshing algorithm in §2 to determine a conforming mesh for Ω. We assume that the background mesh $\mathcal{T}_h$ is specified by (i) a list of

coordinates V of its vertices, (ii) a numbering I for the vertices, and (iii) a list of triangle connectivities C which are 3-tuples of vertex numbers. Vertex with number $i \in I$ is denoted $v_i \in V$. A triangle with vertices $\{v_i, v_j, v_k\}$ has connectivity $(i, j, k) \in C$. The algorithm returns a conforming triangulation for Ω specified by a set of vertices V^Ω, a numbering $I^\Omega \subseteq I$ for these vertices and a connectivity list $C^\Omega \subseteq C$ for triangles in the mesh.

Require: vertex coordinates V, vertex numbering I, triangle connectivities C.
Require: Choose $\eta \in (0, 1)$ and r equal to a few multiples of h

Initialize $I^\Omega \leftarrow \emptyset, V^\Omega \leftarrow \emptyset, C^\Omega \leftarrow \emptyset$
for all $i \in I$ **do**
    if $v_i \in \Omega$ **then**
        $s_i \leftarrow$ true
    else
        $s_i \leftarrow$ false
    end if
    if s_i **then**
        Append i to I^Ω
        if $-r < \phi(v_i)$ **then**
            Append $\mathfrak{p}_h(v_i)$ to V^Ω
        else
            Append v_i to V^Ω
        end if
    end if
end for
$I^+ \leftarrow \emptyset$
for all $(i, j, k) \in C$ **do**
    $\mathfrak{i}_- \leftarrow \emptyset, \mathfrak{i}_+ \leftarrow \emptyset$
    for $\ell \in \{i, j, k\}$ **do**
        if s_ℓ **then**
            Append ℓ to $\mathfrak{i}_-$
        else
            Append ℓ to $\mathfrak{i}_+$
        end if
    end for
    if $\#\mathfrak{i}_- \geq 1$ **then**
        Append (i, j, k) to C^Ω
        if $\#\mathfrak{i}_+ = 2$ **then**
            Ensure conditioning angle of triangle (i, j, k) is acute.
            for $\ell \in \mathfrak{i}_+$ **do**
                Append ℓ to I^+
            end for
        end if
    end if
end for
for all $i \in I^+$ **do**
    Append i to I^Ω
    Append $\pi(v_i)$ to V^Ω
end for
return triangulation $(V^\Omega, I^\Omega, C^\Omega)$ for Ω